

## **MSG/SEVIRI SOLAR CHANNEL CALIBRATION**

The document presents a vicarious calibration method based on calculated radiances that will be applied to the solar channels of the Spinning Enhanced Visible and Infrared Imager instrument on-board Meteosat Second Generation satellites. This paper has been presented at the 33rd COSPAR Scientific Assembly, Warsaw, Poland, 16 – 23 July 2000.

# OPERATIONAL VICARIOUS CALIBRATION OF THE MSG/SEVIRI SOLAR CHANNELS

*Y.M. Govaerts, A. Arriaga and J. Schmetz*

EUMETSAT, Am Kavalleriesand 31  
D-64295 Darmstadt, Germany

## 1 Introduction

Meteosat Second Generation (MSG) is a new series of European geostationary meteorological satellites operated by EUMETSAT. The MSG programme consists of at least three satellites each with an expected lifetime of seven years. MSG is a spinning satellite and carries a twelve channel imager, called SEVIRI (Spinning Enhanced Visible and Infrared Imager) with 11 spectral channels located between  $0.6\mu\text{m}$  and  $14\mu\text{m}$  and a high resolution visible channel (HRV). The characteristics of SEVIRI are briefly described in the next Section.

The SEVIRI spectral observations distributed across the solar and infrared part of the electro-magnetic spectrum combined with the 15 minutes repeat cycle will provide the basis for improved or new geophysical products, that will be used for applications such as numerical weather prediction and climate monitoring. The retrieval of quantitative geophysical parameters requires however the absolute calibration of the spectral channels, and the monitoring of sensor behaviour. An on-board black body calibration mechanism will ensure the thermal channel calibration with an accuracy better than 1 K. No on-board device will be available for the calibration of SEVIRI solar channels. Hence, the calibration of these channels will have to rely on vicarious calibration methods. Various approaches have been proposed for the calibration of the solar channel of the current Meteosat radiometer. So far, none of these methods have been used on an operational basis, although this has been proven to be feasible for the thermal channels (Schmetz 1989; Gube et al. 1996).

The proposed vicarious calibration method relies on radiative transfer modelling over bright desert, sea and optically thick cloud targets. This method should provide a calibration accuracy better than 5% during the entire MSG mission lifetime accounting for the constraints of an operational environment. In this context, the estimation of the calculated radiance error is a key factor that determines the calibration accuracy. The radiative transfer modelling error due to calibration target characterisation errors is firstly investigated. In order to reduce the error of the simulated top-of-atmosphere (TAO) radiance over the selected calibration targets, several hundred images are processed for the derivation of the calibration coefficients. In addition, automatic quality control mechanisms have been developed to verify the consistency of the results. These quality control mechanisms provide a robust calibration scheme that can be used on an operational basis during the entire lifetime of the MSG mission, *i.e.*, more than 12 years. The results achieved so far with the current Meteosat satellite have shown that an absolute calibration coefficient can be computed within an error below 10% over sea and desert targets.

## 2 The seviri radiometer

SEVIRI is the main radiometer on-board the MSG spacecraft. The characteristics of its spectral band are given in Table 1, where the actual pre-launch radiometric performance are given for the MSG-1 satellite. Each spectral channel has three detectors, except HRV with nine. The medium-term (long-term) drift of the solar channels should be better or equal to 0.1% (2%) of the dynamic range. The normalised spectral response of the solar channels are characterised with a mean relative error of about 1%. The East-West and North-South

sampling rate at the sub-satellite point is  $3 \times 3$  km ( $1 \times 1$  km for HRV), and the instantaneous field of view is about 5km (2km for HRV).

Channel	Spectral Band ( $\mu\text{m}$ )	Dynamic Range	Short-term Noise Require.	Short-term Noise Perform.	SSR std. dev.
HRV	silicon response	$0 - 460 \text{ W m}^{-2} \text{ sr}^{-1} \mu\text{m}^{-1}$	$\text{SNR} > 4.3$	$\text{SNR} > 4.6$	1.8%
VIS0.6	0.56 – 0.71	$0 - 533 \text{ W m}^{-2} \text{ sr}^{-1} \mu\text{m}^{-1}$	$\text{SNR} > 10.1$	$\text{SNR} > 14.3$	1.0%
VIS0.8	0.74 – 0.88	$0 - 357 \text{ W m}^{-2} \text{ sr}^{-1} \mu\text{m}^{-1}$	$\text{SNR} > 7.3$	$\text{SNR} > 9.7$	1.0%
NIR1.6	1.50 – 1.78	$0 - 75 \text{ W m}^{-2} \text{ sr}^{-1} \mu\text{m}^{-1}$	$\text{SNR} > 3.0$	$\text{SNR} > 3.0$	0.5%

Table 1: SEVIRI solar channel characteristics. The Signal to Noise Ratio (SNR) is given at 1% of the maximum dynamic range. The standard deviation (std. dev.) of the Sensor Spectral Response (SSR) characterisation error is given in percent.

The radiometric pre-processing of level 1.0 data, *i.e.*, the transformation of raw data to level 1.5 geo-located data, will include the linearisation of the signal, equalisation of the detector output of a same channel and finally pixel geo-location to a reference grid. An on-board black body calibration mechanism coupled with the simulation of the front optics contribution should ensure an absolute calibration accuracy of the infrared channels better than 1K. SEVIRI data will be geo-located with an absolute accuracy of 1 pixel and a root mean square error from image to image less than 0.5 pixel. Ground control points will be used to monitor the quality of the geo-location process. When the level 1.5 data are generated, pixels from the three (nine) detectors are re-sampled to the reference grid, so that it is not possible anymore to associate afterwards a specific detector to each rectified pixel. The proposed calibration approach relies on SEVIRI level 1.5 data.

### 3 Review of past meteosat visible band calibration approaches

Vicarious absolute calibration methods rely on an independent estimation of the radiances observed by the radiometer. For Meteosat first generation, three different techniques have essentially been used for the estimation of the incoming radiance in the visible spectral region: (i) instrument cross-calibration, (ii) airborne calibration campaign, and (iii) radiative transfer modelling.

The first method is meaningful only if at least one of the two instruments has an accurate on-board calibration device. It also requires that observations from the two instruments are acquired over the same area (same footprint), at the same time, and within the same spectral range and viewing geometry. With exception for pointing device or multi-angular instruments, such conditions can hardly be met between geostationary and polar orbiting satellites (*e.g.*, Marshall et al. 1999). Such method has however already been used for the calibration of the Meteosat solar channel (*e.g.*, Cabot et al. 1994; Rossow et al. 1996). Both methods are based on cross-calibration with bands 1 and 2 of the NOAA/AVHRR instrument, which have no on-board calibration device. Observations from enhanced radiometers with on-board calibration (*e.g.*, ATSR, MISR) are now available, but these instruments will not be available during the entire MSG mission. It is therefore difficult to apply this approach on a regular basis and for a consistent sensor drift monitoring, although it may be relevant for validation purposes.

Calibration campaign has been the main method adopted by EUMETSAT for the calibration of the Meteosat solar channel (Kriebel and Amann 1993). These authors derived a calibration coefficient comparing Meteosat observations with data from a similar calibrated airborne radiometer over four different targets. The estimated calibration error is  $\pm 5\%$ . This method is however too expensive to be used on a regular basis for monitoring the sensor drift and it cannot be envisaged as the primary SEVIRI operational calibration method. It is an interesting method for the validation of an operational calibration method.

Koepke (1982) has been the first author to propose the use of calculated top-of-atmosphere radiance and observed surface bidirectional reflectances for the calibration of the Meteosat instrument. He took advantage of different surface reflectances to derive independent count/radiance relations. It is an attractive method with

an estimated error of  $\pm 6\%$ . This method can be used for monitoring the sensor gain drift over a long period at very low cost, as proven by Moulin et al. (1996). These previous studies thus showed that calculated radiances can be used to derive absolute calibration coefficient on a regular basis with an accuracy comparable to the one from airborne campaigns.

Our objective is to derive calibration coefficients based on calculated radiance with an accuracy better than 5% during the entire MSG mission. In order to achieve this objective, two key factors need to be investigated: the estimation of the calculated radiance error and the control of the calibration consistency. This control requires the processing of a large amount of images and the use of targets with spectrally different properties. The issue of target characterisation accuracy is addressed in the next section.

## 4 Calibration target characterisation

The spectral radiance  $R(\lambda)$  impinging on the detectors is determined by a set of independent parameters  $\{\Omega, t, x, \Delta_\lambda\}$  that define the observation conditions and a set of state variables  $\{\chi_P\}$  that describe the properties of the observed targets.  $\Omega$  represents the sun and viewing angles,  $t$  is the time of observation,  $x$  is the location of the target and  $\Delta_\lambda$  is the spectral band, *i.e.*, the sensor spectral response. The time and angles of observation can be determined accurately, so that only the errors on  $x$  and  $\Delta_\lambda$  are to be considered. In case of homogeneous targets, the error on  $x$ , about 0.5 pixel, can be neglected so that only the error on the sensor spectral response, given in Table 1, should actually be taken into account. It will however be neglected in the present analysis.

Each variable  $\{\chi_p\}$  (with  $p = 1, \dots, P$ ) that characterises the target outgoing radiance is known with an error  $\varepsilon_p$ . The resulting radiance error  $\delta R_P(\lambda)$  can be estimated as suggested by Arriaga and Schmetz (1999)

$$\delta R_P(\lambda) = \sqrt{\sum_{p=1}^P \left| \frac{\delta(R(\lambda))}{\delta\chi_p} \right|_{\chi_j \neq p}^2 \varepsilon_p^2}. \quad (1)$$

The partial derivative of the outgoing radiance  $\delta R/\delta\chi_p$  with respect to the parameter  $\chi_p$  represents the sensitivity of the spectral radiance  $R(\lambda)$  (for a specified set of independent parameters  $\{\Omega, t, x, \Delta_\lambda\}$ ) solely due to small perturbations in the model parameter  $\chi_p$ , all other parameters  $\chi_j$  remaining unperturbed.

Since the value of calibration coefficient derived over spectrally different target types should be the same, the consistency of the calibration coefficients can thus be verified by comparing the coefficients obtained with these different target types. The values of  $\delta R_p(\lambda)$  will indeed be affected by independent sources of error. These errors have been investigated over sea surfaces, bright deserts and high level opaque clouds. The corresponding TOA spectral radiances  $R(\Omega, t, x, \lambda; \chi_P)$  are computed with the 6S model (Vermote et al. 1997) over sea and desert and the Matrix Operator Method (MOM) radiative transfer model (Liu and Ruprecht 1996) over clouds.

### 4.1 Sea Surface

The aerosol optical thickness and surface wind speed are the two main state variables that govern the TOA radiance over sea surfaces in the SEVIRI solar bands. The ocean colour, total column water vapour and ozone contribute also to the observed radiances, but only to a lesser extend. The error can be minimised selecting targets with low wind speed and aerosol load, avoiding sun glint conditions. An area in the South Atlantic, near  $15^\circ\text{S}$  and  $25^\circ\text{W}$ , has been selected for the estimation of a typical radiance error. The corresponding viewing zenith angle is about  $30^\circ$ , and sun zenith angles at local noon varies from  $10^\circ$  in Winter to  $30^\circ$  in Summer. The parameter values used for the error estimation are given in Table 2.

The corresponding effective radiance (see Eq. 2) of the four SEVIRI solar channels is given in Table 3. Outside the sun glint region, most of the error is due to the error on the aerosol optical thickness characterisation, whereas the wind speed errors dominates within this region. The error on the total ozone is maximum in the

Parameter	Unit	Sea	Desert	Cloud
Sun Zenith Angle	degree	30	30	0
Viewing Zenith Angle	degree	30	40	0
Relative Azimuth	degree	45	90	0
Total Ozone	DU	$320 \pm 10$	$320 \pm 10$	—
Total Water Vapour	$\text{kg m}^{-2}$	$20 \pm 5$	$20 \pm 2.5$	—
Wind Speed	$\text{ms}^{-1}$	$3 \pm 2$	—	—
Aerosol Type		Maritime	Desert	—
Aerosol Optical Thickness at $0.55\mu\text{m}$		$0.05 \pm 0.0125$	$0.2 \pm 0.05$	—
Cloud Optical Thickness		—	—	$90 \pm 30$

Table 2: Values of the state variables and angular configurations for the error estimation over the three target types.

VIS0.6 band, but does not exceed 0.5% of the total signal. The maximum error from the total column water vapour occurs in the VIS0.8 band, although it does not exceed 0.5% of the simulated radiance. For the HRV and VIS0.6 bands, the total error is lower than 5%, whereas the VIS0.8 band is quite sensitive to the error on the aerosol optical thickness. In the NIR1.6 band, the ratio between the effective radiance and the estimated error is similar to the SNR. Sea targets cannot therefore be used for the calibration of this band.

Target	Value ( $\text{Wm}^{-2}\text{sr}^{-1}\mu\text{m}^{-1}$ )	HRV	VIS0.6	VIS0.8	NIR1.6
Sea	Radiance	14.4	13.7	4.4	0.2
	Radiance Error	0.5	0.6	0.4	0.06
	Relative Error (%)	3.5	4.4	9.1	30.0
Desert	Radiance	111.5	136.3	110.8	29.0
	Radiance Error	6.3	7.9	6.9	1.8
	Relative Error (%)	5.7	5.8	6.2	6.2
Cloud	Radiance	459.3	525.2	362.5	14.3
	Radiance Error	27.8	29.9	15.8	<.1
	Relative Error (%)	6.1	5.7	4.4	<.1

Table 3: Typical calculated radiance error over the three target types for the SEVIRI solar channels.

## 4.2 Bright Desert

To estimate a typical radiance error over bright desert, a sand dune site located in Egypt (22.8°N, 26.8°E) has been selected. The SOILSPEC model (Jacquemoud et al. 1992) has been inverted against the surface bidirectional reflectance factor derived from POLDER observations (Bicheron and Leroy 2000). The retrieved model parameters have been spectrally interpolated to the SEVIRI bands, forcing the albedo to match a bright sand spectrum. The error on the surface bidirectional properties are assumed to be 2.5% for the single scattering albedo of the sand particles and 10% for the Legendre polynomial coefficients of the phase function. The same error has been assumed for the hot spot parameter. The value of the other parameters are given in Table 2.

Results are shown in Figure 1. For all bands, the error is in the range of 5 – 6 % of the signal (Table 3). This error is dominated by the error on the single scattering albedo and by the error on the surface anisotropy. The error from the aerosol optical thickness has an impact lower than 1%. Note that error due to inappropriate aerosol type may introduce an error larger than the error on the aerosol optical thickness. This effect has however not been investigated in detail in the present study.

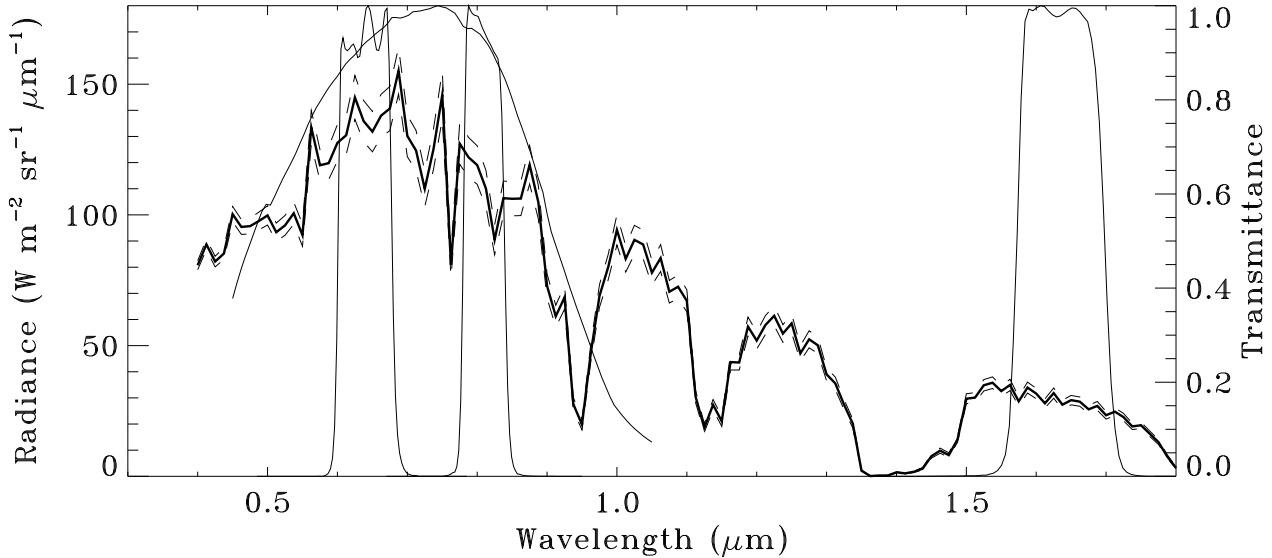


Figure 1: Outgoing radiance over the selected desert target for the specified state variables (thick line). The estimated error is shown with the dashed lines. The spectral response of the four SEVIRI solar channels is indicated with thin solid lines.

### 4.3 High Level Opaque Cloud

Cloud calibration target type has been selected in order to cover the full dynamic range of the instrument. As can be seen from Figure 2, the effective TOA radiance over high tropical cumulonimbus clouds increases slowly with the optical thickness and almost saturates for optical thicknesses above 100. For the time being, only the impact of the uncertainty on the cloud optical thickness is explored, assuming no error in the characterisation of the cloud micro-physical properties.

The micro-physical properties of high tropical cumulonimbus clouds composed of water and ice phases are taken from ISCCP (Rossow et al. 1991). The effective radius of cloud and ice particles is fixed to  $10\mu\text{m}$  and  $25\mu\text{m}$  respectively. Cloud optical thicknesses at  $0.550\mu\text{m}$  have been simulated on the basis of 50% of liquid water between 1.5 and 10 km and 50% of ice between 5km and 15km. The issue concerning the identification of such cloud is addressed in the next section.

For the current error estimation, a cloud located at the sub-satellite point is simulated with an optical thickness of  $90 \pm 30$ . As can be seen from Table 3, the corresponding radiances are close to the maximum dynamic range of the SEVIRI channels in the visible and near-infrared region. The respective error is about 5%, but for the NIR1.6 band whose radiance saturated and is therefore not sensitive to any error in the optical thickness. This latter band is however expected to be very sensitive to error in the description of the phase and effective radius of the cloud particles.

## 5 Operational calibration method

In order to reduce the uncertainty on the calibration coefficient estimation and control the consistency of the results, the SEVIRI solar channel calibration scheme relies on the processing of a large amount of images during a period  $[p_1, p_2]$  of typically 10 days. The objective is to detect inconsistent results, if any, and to assign an error on the estimated calibration coefficients. It is intended to derive these coefficients on a regular basis. To this end, a calibration algorithm that automatically acquires the required input data and analyses the SEVIRI data is currently being developed at EUMETSAT. The main processing steps of this algorithm are described in

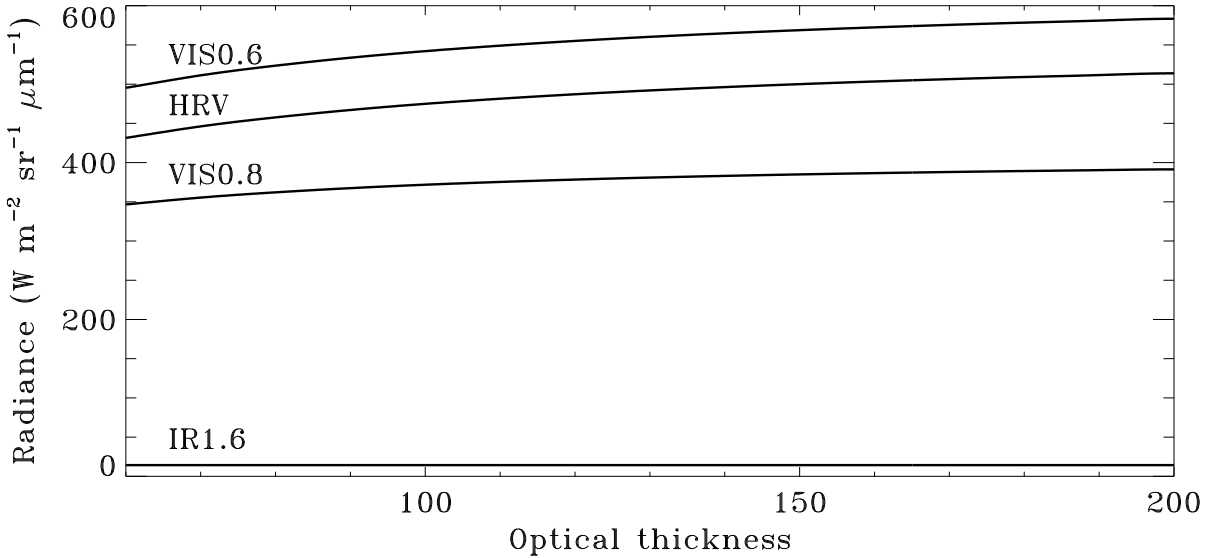


Figure 2: Effective TOA radiance in the four SEVIRI solar channels over tropical cumulonimbus clouds as a function of the optical thickness at  $0.55\mu\text{m}$ . Sun and viewing zenith angles are set to  $0^\circ$ . The pressure at the cloud top high is 140 hPa.

this section.

## 5.1 Target Identification

For each analysed image during the period  $[p_1, p_2]$ , a target identification process takes place over each target type. This identification process relies, among other, on the output of the operational SEVIRI cloud analysis scheme developed at EUMETSAT (Lutz 1999). The purpose of this processing step is to select targets whose actual properties and observation/illumination angles correspond to cases where the calculated radiance error is minimum.

Sea targets are defined by a large search area in which a small window of  $N_c \times N_l$  cloud free pixels is searched for uniform and very low digital count values. This test is used to ensure a very low aerosol optical thickness. When such a window has been identified, the angular configuration is checked, rejecting sun-glint cases. The values of the surface wind speed and the total column water vapour are extracted next from ECMWF data. The window is disregarded when the wind speed exceeds  $10\text{ms}^{-1}$ . In case several windows fulfil the identification conditions within the search area, the darkest one is selected. Over desert, the targets, listed in Cosnefroy et al. (1996), are flagged as “identified” when they are cloud free. High level opaque clouds are searched in the tropical region close to the sub-satellite point on the basis of the cloud analysis results. The identification mechanism searches for pixels classified as 100% cloudy, opaque, ice phase, with the top higher than 150 hPa. Sun and viewing zenith angles above  $20^\circ$  are avoided.

## 5.2 Pixel Value Extraction

Once a target has been identified, the digital count values are extracted from the corresponding image. To minimise the effects of image geo-location errors and to make sure that all detectors of a band contribute to the identified target, the  $N_l \times N_c$  pixels surrounding the target centre are extracted. The mean count value  $\widehat{K}(t)$  and associated error  $\delta\widehat{K}(t)$  are estimated next.

### 5.3 Radiative Transfer Modelling

The incoming and effective radiance is calculated over the identified targets for the illumination and viewing angles  $\Omega$  at the time  $t$  of observation and the surface and atmospheric properties  $\chi_P$  of the target. The effective radiance  $\tilde{R}_f$  is computed accounting for the normalised spectral response  $\xi(\lambda)$  of each SEVIRI solar spectral band

$$\tilde{R}_f(\Omega, t, x; \chi_P) = \frac{\int_{\lambda} R(\Omega, t, x, \lambda; \chi_P) \xi(\lambda) d\lambda}{\int_{\lambda} \xi(\lambda) d\lambda}. \quad (2)$$

The estimation of  $\tilde{R}_f(\Omega, t, x; \chi_P)$  is however affected by the error  $\varepsilon_P$  of  $\chi_P$  and the error  $\delta\xi(\lambda)$  of the sensor spectral response. The error  $\delta\tilde{R}_f(\Omega, t, x; \chi_P)$  of the effective radiance  $\tilde{R}_f(\Omega, \chi_P)$  is therefore also calculated as a function of the error  $\delta R_P(\lambda)$  calculated with Eq. 1 and the error  $\delta\xi(\lambda)$  on the sensor spectral response characterisation.

### 5.4 Calibration and Quality Control

For each SEVIRI band, a calibration coefficient  $c_f(t)$  is estimated for every identified targets as

$$c_f(t) = \frac{\tilde{R}_f(\Omega, t, x; \chi_p)}{\widehat{K}(t) - K_0(t)}. \quad (3)$$

where  $K_0(t)$  is the digital count offset. The corresponding estimated error is calculated with

$$\delta c_f(t) = c_f(t) \sqrt{\left| \frac{\delta \tilde{R}_f(\Omega, t, x; \chi_p)}{\tilde{R}_f(\Omega, t, x; \chi_p)} \right|^2 + \left| \frac{\delta \widehat{K}(t)}{\widehat{K}(t) - K_0(t)} \right|^2 + \left| \frac{\delta K_0(t)}{\widehat{K}(t) - K_0(t)} \right|^2}. \quad (4)$$

The inverse squared error  $\kappa_c(t) = 1/|\delta c_f(t)|^2$  is used as a weight to calibration coefficient  $c_f(t)$ .

Over a desert target, the consistency of the daylight cycle representation is first controlled (Govaerts et al. 1998). This test exploits the non-linear dynamic count variations due to changing illumination conditions. These count values, when combined with the simulated radiances, should form a straight line. The intersection of this line with the null radiance line should provide an estimation of the space count  $\overline{K}'_0$ , that can be compared with the actual mean value over the same period  $\overline{K}_0$ . When the retrieved value  $\overline{K}'_0$  differs from the observed value  $\overline{K}_0$  more than the quadratic sum of their respective errors, the corresponding target is disregarded for the estimation of the final calibration coefficient.

The coefficients  $c_f(t)$  derived over a same target during the period  $[p_1, p_2]$  are next combined. Extreme values of  $c_f(t)$  are first rejected and a weighted mean calibration coefficient  $\bar{c}_f$  is computed over each calibration target with the remaining coefficients. The dispersion of these mean calibration coefficients  $\bar{c}_f$  derived over a similar target type is analysed, rejecting extreme values of  $\bar{c}_f$ . The mean value  $(\bar{c}_{f,SEA}, \bar{c}_{f,DESERT}, \bar{c}_{f,CLOUD})$  is evaluated over each target type, *i.e.*, sea, desert and cloud, using the targets which have not been disregarded so far in the calibration process. Assuming that the detector response is linear and that the characterisation of the sensor spectral response is correct, these three coefficients should be similar within their respective errors (Govaerts 1999). The final calibration coefficient is the weighted mean value of all the valid coefficients  $c_f(t)$ .

## 6 First results

The proposed method has been evaluated against Meteosat 7 data for a period running from 1 up to 10 January 1999. Sea target search areas are located in the South Atlantic, from  $30^{\circ}\text{W}$  up to  $15^{\circ}\text{W}$ , and from  $5^{\circ}\text{S}$  up to  $15^{\circ}\text{S}$ . The desert target location is listed in Cosnefroy et al. (1996). Cloud targets corresponding to high level opaque clouds are search within an area limited to  $35^{\circ}\text{N}$  and  $35^{\circ}\text{S}$  and,  $30^{\circ}\text{W}$  and  $30^{\circ}\text{E}$ . Over sea targets, slots

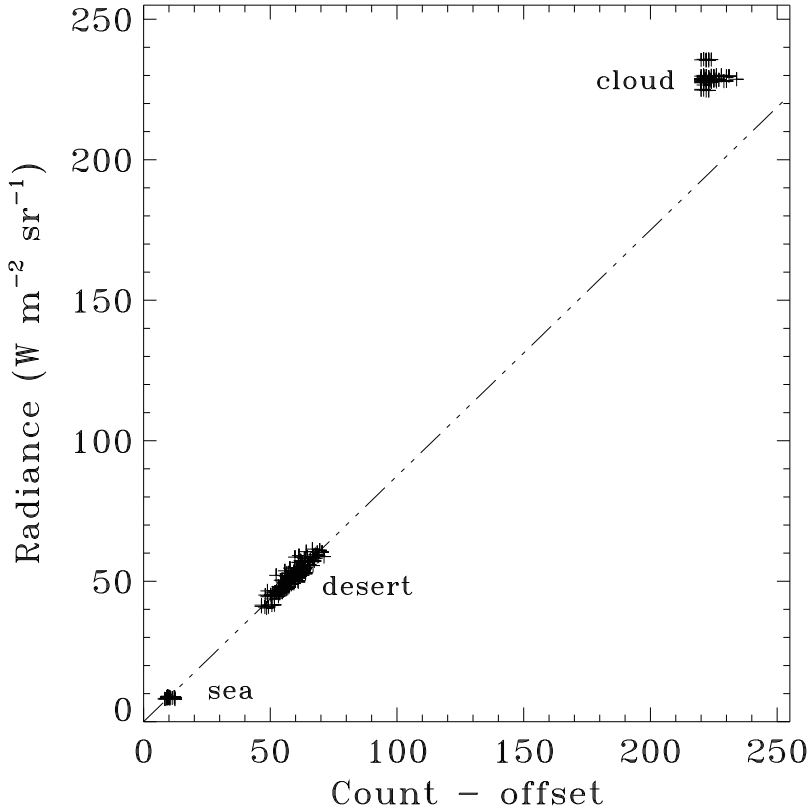


Figure 3: Scatter plot of the observed count minus the space count versus the simulated effective radiance.

23 to 30 have been used (*i.e.*, from 11:30UT to 15:00UT) while slots 10 to 36 have been used over desert targets. Cloud target identification has been restricted to slot 24.

ECMWF data have been used for the estimation of the total column water. Total ozone climate data is taken from Total Ozone Mapping Spectrometer (TOMS) instrument observations. Over sea, maritime aerosol are assumed with a mean aerosol optical thickness of 0.05 at  $0.55\mu\text{m}$ . Desert aerosol is assumed over the Sahara region, with a mean optical thickness of 0.2 at  $0.55\mu\text{m}$ . The cloud analysis has been performed with the MSG prototype code adapted to the processing of Meteosat data. Due to the lack of information on the actual optical thickness  $\tau_c$  of the identified cloud targets, the value  $\tau_c$  that minimises the following merit function

$$f(\tau_c) = \sqrt{\sum_t \left( \frac{\tilde{R}_f(\tau_c)/\bar{c}_{f,CLOUD}(\tau_c) - (\hat{K}(t) - K_0(t))}{\kappa_c(t, \tau_c)} \right)^2} \quad (5)$$

has been selected, which occurs at  $\tau_c = 120$ .

40 targets have been successfully identified within the sea search areas. The mean coefficient  $\bar{c}_{f,SEA} = 0.86 \pm 0.042 \text{Wm}^{-2}\text{sr}^{-1}/\text{count}$  has been derived during that period. Among the 19 desert calibration targets, only five have actually been used. The other ones have been rejected as they were too cloudy, the daylight fit test failed or their mean value  $\bar{c}_f$  too far from the overall value  $\bar{c}_{f,DESERT}$ . The resulting coefficient  $\bar{c}_{f,DESERT}$  is equal to  $0.87 \pm 0.012 \text{Wm}^{-2}\text{sr}^{-1}/\text{count}$ . These two first coefficients are in good agreement. Over the 81 identified cloud targets, the coefficient  $\bar{c}_{f,CLOUD} = 1.03 \pm 0.018 \text{Wm}^{-2}\text{sr}^{-1}/\text{count}$  has been derived. This value overestimates by 18% the coefficient derived over sea and desert target types as can be seen in Figure 3. This discrepancy may result from several factors. First, the radiative transfer model does not account for the actual three dimensional structure of cumulonimbus clouds, that may translate into an overestimation of the actual radiance. Second, the sensor spectral response of Meteosat instrument visible band has been measured only

between  $0.5\mu\text{m}$  and  $0.9\mu\text{m}$  and extrapolated outside this interval. The radiance peak occurs around  $0.5\mu\text{m}$ , so that the value of the effective radiance may have been overestimated. Finally, the mean values of the cloud micro-physical properties should be re-evaluated.

## 7 Conclusions

The proposed calibration method relies extensively on radiative transfer computations over a series of targets during a 10 day period. The quality control mechanisms allow to reduce the calibration error by rejecting inconsistent results. The estimated calibration accuracy is close to 5% for the Meteosat 7 instrument over sea and desert target types. The calibration coefficient derived over cloud target type seems overestimated. The reasons of this discrepancy still need to be further investigated.

This method will be applied on a regular basis to the calibration of the solar channels of SEVIRI and will benefit from several improvements. For instance, the aerosol optical thickness characterisation could be improved by using products derived from the MISR instrument on the Terra platform (Martonchik 1997). Over cloud targets, it is expected that the result of the scene analysis will benefit from the enhanced spectral resolution of SEVIRI and provide therefore more reliable results. In particular, the exploitation of the difference between the VIS0.8 and NIR1.6 bands will help the estimation of the cloud particles mean radius.

## References

- Arriaga, A. and J. Schmetz, Calibration of the Meteosat-5/-6 VIS channels with help of modelled radiances, *Contrib. Atmos. Physics*, **72**, 133 (1999).
- Bicheron, P. and M. Leroy, BRDF signatures of major biomes observed from space, Submitted to *JGR*.
- Cabot, F., G. Dedieu, and P. Maisongrande, Monitoring NOAA/AVHRR and Meteosat shortwave bands calibration and inter calibration over stable areas, in *Physical Measurements and Signatures in Remote Sensing, Proceedings of the 6th ISPRS Symposium*, Val d'Isere, France, pp. 41–46 (1994).
- Cosnefroy, H., M. Leroy, and X. Briottet, Selection and characterization of Saharan and Arabian desert sites for the calibration of optical satellite sensors, *Rem. Sens. Environ.*, **58**, 101 (1996).
- Govaerts, Y. M., Correction of the Meteosat-5 and -6 VIS band relative spectral response with Meteosat-7 characteristics, *Int. J. Rem. Sens.*, **20**, 3677 (1999).
- Govaerts, Y. M., B. Pinty, M. M. Verstraete, and J. Schmetz, Exploitation of angular signatures to calibrate geostationary satellite solar channels, in IEEE (Ed.), *IGARSS'98*, Seattle, USA, pp. 327–329 (1998).
- Gube, M., V. Gaertner, and J. Schmetz, Analysis of the operational calibration of the Meteosat infrared-window channel, *Meteorol. Applied*, **3**, 307 (1996).
- Jacquemoud, S., F. Baret, and J. F. Hanocq, Modelling spectral and bidirectional soil reflectance, *Rem. Sens. Environ.*, **41**, 123 (1992).
- Koepke, P., Vicarious satellite calibration in the solar spectral range by means of calculated radiances and its application to Meteosat, *Ap. Opt.*, **21**, 2845 (1982).
- Kriebel, K. T. and V. Amann, Vicarious Calibration of the Meteosat visible channel, *Journal of Atmospheric and Oceanographic Technology*, **10**, 225 (1993).
- Liu, Q. and E. Ruprecht, Radiative transfer model: matrix operator method, *Ap. Opt.*, **35**, 4229 (1996).
- Lutz, H. J., Scenes and cloud analysis for Meteosat Second Generation, Technical Report 4, EUMETSAT (1999).
- Marshall, J. F. L., J. J. Simpson, and Z. Jin, Satellite calibration using a collocated nadir observation technique: theoretical basis and application to the GMS-5 pathfinder benchmark period, *IEEE Trans. Geo. Rem. Sens.*, **37**, 499 (1999).
- Martonchik, J. V., Determination of aerosol optical depth and land surface directional reflectances using multiangle imagery, *JGR*, **102**, 17014 (1997).
- Moulin, C., C. E. Lambert, J. Poitou, and F. Dulac, Long term (1983-1994) calibration of the Meteosat solar (VIS) channel using desert and ocean targets, *Int. J. Rem. Sens.*, **17**, 1183 (1996).

- Rossow, W. B., C. L. Brest, and M. D. Roitier, International satellite cloud climatology project (ISCCP): New radiance calibrations, Technical Report WMO/TD-No 736, WMO (1996).
- Rossow, W. B., L. C. Garder, P. J. Lu, and A. W. Walker, International satellite cloud climatology project (ISCCP): Documentation of cloud data, Tech. Doc. WMO/TD 266, 76 pp., WMO (1991).
- Schmetz, J., Operational calibration of the Meteosat water vapour channel by calculated radiances, *Ap. Opt.*, **28**, 3030 (1989).
- Vermote, E. F., D. Tanré, J. L. Deuzé, M. Herman, and J. J. Morcrette, Second simulation of the satellite signal in the solar spectrum, 6S: An overview, *IEEE Trans. Geo. Rem. Sens.*, **35**, 675 (1997).